Bilayer thin films based on $K_3Bi_2I_9$/MO (M=Ti, Zn, and Cu) for CO_2 photoreduction

E. Luévano-Hipólito, O.L. Quintero-Lizárraga, M.R. Alfaro-Cruz, L.I. Ibarra-Rodríguez, L.M. Torres-Martínez

This work reports the fabrication of bilayer thin films of $K_3Bi_2I_9$/MO (M=Ti, Cu, Zn) as an extrinsic strategy to enhance the stability of lead-free metal halide perovskite (LFMHPs) for CO_2 photoreduction. The perovskites were grown on mica substrates by the spin-coating technique, which serves as a seed layer for the deposition of TiO_2, ZnO, and CuO oxides by physical (sputtering) and chemical (atomic layer deposition) techniques. The $K_3Bi_2I_9$/MO samples exhibited enhanced light absorption and better stability than the reference $K_3Bi_2I_9$ perovskite. Despite the efficiency of the bilayer films was lower than the reference ($K_3Bi_2I_9$) for CO_2 photoreduction, the $K_3Bi_2I_9$/CuO arrangement favored better stability and efficiency. These results provide an alternative to design new and more stable optical devices for photocatalytic applications.

Introduction

CO_2 photoreduction

The CO_2 reduction by heterogeneous photocatalysis is based on its conversion towards value-added products or renewable solar fuels, commonly known as "artificial photosynthesis" due to its similarity with natural photosynthesis present in the biological fixation of CO_2 [1]. This process requires CO_2, H_2O, sunlight, and a photocatalyst (a semiconductor material) to generate solar (and renewable) fuels. The reaction mechanism of the CO_2 photoreduction starts when the photocatalyst is excited by an external energy (ideally, sunlight) of equal or higher value than its band gap energy. Then, this excitation promotes the transfer of electrons from the valence band (VB) to its conduction band (CB), simultaneously generating electrons (e^-) and holes (h^+) capable of oxidizing the adsorbed species, e.g., water to produce reducing species (H^+) that react with the CO_2 molecule to generate different oxygenated products (CO, HCOOH, HCHO, CH_3OH) and short-chain olefins (C_2H_4, C_3H_6) [2]. The efficiency and the selectivity of this reaction will depend on several factors, among which the type of photocatalyst stands out [3], which includes oxide and non-oxide, sulfides, molecular catalysts, and other/diverse catalysts [4]. Among them, the materials with perovskite structures, mainly metal halide perovskites, had promoted high efficiencies for CO_2 reduction, mainly to produce CO and CH_4 [5, 6].

Lead-free metal halide perovskites

Metal halide perovskites (MHP) are recognized as an ideal choice for CO_2 photoreduction owing to their outstanding optoelectronic properties such as light absorption coefficient, tunable bandgap, superior defect tolerance, long carrier diffusion length, and remarkable quantum efficiency. These favorable properties have been used to design different photosystems, e.g., photovoltaic, photodetectors, light-emitting diodes, and, recently, as photocatalysts. Remarkably, the application of MHP in solar cells has shown the rapid improvement of the power conversion efficiency from 3.8 to 25.2% in the last years [6]. Inspired by the excellent properties of MHPs, the study of their photocatalytic activity for CO_2 reduction to generate renewable solar fuels has recently attracted much attention.

So far, cesium lead bromide ($CsPbBr_3$) is the MHP with the highest yield reported for CO and CH_4 production (431 μmol g^{-1} h^{-1}) of this group of materials [7]. Despite the promising activity of MHPs for CO_2 photoreduction, lead in its structure entails environmental toxicity problems. Thus, numerous efforts have been made to replace this metal without sacrificing its good performance by developing lead-free metal halide perovskites (LFMHPs). One example is the replacement of Pb by trivalent cations that allow the formation of new stoichiometries, such as $A_3B_2X_9$ (A=Cs, K, B=Bi, Sn, X=I, Br, Cl) stoichiometry. Among these materials, the use of the Cs^+ and Bi^{3+} cations in the A and B sites, respectively has resulted in outstanding efficiencies for CO and CH_4 production from CO_2 photoreduction, with the $Cs_3Bi_2I_9$ perovskite [8]. Recently, our research group demonstrated that alternative formulations are possible by the replacement of Cs^+ with K^+ to give place to the formation of $K_3Bi_2X_9$ perovskites with promising activity to produce liquid solar fuels, e.g., HCOOH from CO_2 photoreduction [9]. Although significant efforts have been devoted to designing more effective photocatalysts for CO_2 photoreduction, some issues must be solved before the application of LFMHPs, e.g., charge recombination, instability, and band engineering, to control the selectivity of the reaction.

The band structure of a semiconductor photocatalyst intrinsically controls its CB and VB potential and, thus, influences its activity for different photocatalytic reactions [10]. One method to adapt the band structure is the heterostructure engineering, incorporating additional semiconductors to the photocatalyst. The junction between two or three semiconductors significantly impacts light

E. Luévano-Hipólito ✉, M.R. Alfaro-Cruz
SECIHTI-Universidad Autónoma de Nuevo León, Facultad de Ingeniería Civil- Laboratorio de Ecomateriales y Energía San Nicolás de los Garza, N.L., 66455 México.

O.L. Quintero-Lizárraga, L.M. Torres-Martínez
Universidad Autónoma de Nuevo León, Facultad de Ingeniería Civil-Laboratorio de Ecomateriales y Energía San Nicolás de los Garza, N.L., 66455 México.

L.I. Ibarra-Rodríguez, L.M. Torres-Martínez ✉
Centro de Investigación en Materiales Avanzados, S. C. (CIMAV) Chihuahua, Chih., 31136, México.

Received: October 29th, 2024.
Accepted: December 23rd, 2025.
Published: January 12th, 2026.

https://doi.org/10.47566/2026_syv39_1-260101

absorption, charge transfer efficiency, active sites, the affinity for CO_2 adsorption, and the available redox potentials to control the selectivity of the reaction. Different heterostructures with higher efficiencies than bare materials have been reported with LFMHPs, e.g., $K_3Bi_2I_9$/BiOI [9], $Cs_3Bi_2I_9/Bi_2WO_6$ [11], $Cs_3Bi_2I_9/CeO_2$ [12], $Cs_3Bi_2Br_9/In_4SnS_8$ [13], and other double LFMHPs as $Cs_2AgBiBr_6/TiO_2$ [14]. Also, heterostructure engineering is an efficient strategy for encapsulating the perovskite and improving its efficiency [15]. In this context, the use of simple oxides could represent a good option for designing heterostructures with higher stability in aqueous systems; for example, ZnO is considered a layered window in solar cells to protect the internal semiconductors and, in some cases, could increase the light absorption and improve the transport of the photogenerated charges [16], while CuO has high CO_2 affinity and stability for CO_2 photoreduction [17]. Considering these factors, this work proposes the design of bilayer heterostructures based on $K_3Bi_2I_9$ with TiO_2, ZnO, and CuO to analyze their effect on CO_2 photoreduction efficiency and stability in aqueous solution. The perovskite was deposited by spin-coating on mica substrates; meanwhile, the simple oxides (or encapsulants) by sputtering since a technique that allows good homogeneity on the films.

Experimental

Deposition of $K_3Bi_2I_9$ films

The deposition of the perovskite films was performed by spin-coating. In the first step, an ink of the precursors was synthesized according to a previous report [9]. The method consists of mixed stoichiometric (3:1 molar) amounts of KI (Fermont, 99%) and BiI_3 (Aldrich, 99%) in N,N-dimethylformamide. The ink was sonicated for 15 min and stirred under a magnetic stirrer at 70 °C for 2 h. Then, it was deposited over mica substrates by spin-coating at 2000 rpm for 30 s and annealed at 100 °C for 5 min (Figure 1a).

Encapsulation of $K_3Bi_2I_9$ with metal oxide films

TiO_2, CuO, and ZnO were deposited separately on the $K_3Bi_2I_9$ films by two techniques. A layer of TiO_2 or CuO was grown over the $K_3Bi_2I_9$ surface by DC magnetron sputtering using a metallic Cu and Ti target (99.995% purity, 2.00"×0.250", Kurt J. Lesker). The background pressure of the sputtering chamber was 8×10^{-6} Torr, and the working pressure during deposition was 1.5×10^{-2} Torr. The chamber was filled with argon gas (99.999% purity) and the power used during deposition was 30 W for each target. Afterwards, the bilayer films were calcined at 400 °C for 2 h to promote the oxidation of the metals into CuO and TiO_2 (Figure 1b).

On the other hand, ZnO was deposited by atomic layer deposition (ALD) at 80 °C. The precursors used were DEZ (Diethyl Zinc 95%, STREM Chemicals, CAS 557-20-0) and deionized water. For ZnO deposition it was necessary 500 cycles with the following conditions: 250 ms DEZ, 2 s purge, 250 ms H_2O, and 2 s purge. The registered pressure was 0.9 mbar; these conditions favored a thickness around 100 nm. The methodology used for the deposition and encapsulation of the $K_3Bi_2I_9$ films is shown in Figure 1c.

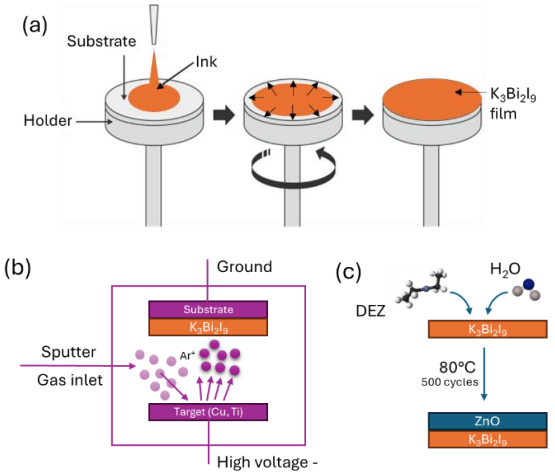

Figure 1. Methodology for the deposition of $K_3Bi_2I_9$ films (a) by spin-coating and their encapsulation by (b) sputtering and (c) atomic layer deposition techniques.

Characterization

The morphological characterization was achieved using Scanning Electron Microscopy (SEM) in a JEOL JSM-6490LV microscope. UV-Visible diffuse reflectance spectroscopy (DRS) was employed to calculate the bandgap energy of the films using an Agilent Technologies UV-Vis-NIR Cary 5000 spectrophotometer equipped with an integrating sphere. The crystal phase was confirmed by X-ray diffraction (XRD) using a PANalytical diffractometer with Cu-Kα radiation.

CO_2 photoreduction assays

The activity of the thin films for CO_2 photoreduction was evaluated at room temperature in a Pyrex glass reactor. For these experiments, one film of 5 cm^2 was used as catalyst. It is worth mentioning that the mass on each film was lower than 0.01 g. The reactor was filled with 100 mL of distilled water under continuous stirring. The reactor was saturated with continuous CO_2 flow and then, a visible lamp (> 400 nm) was turned on outside the reactor. The spectrum of the visible lamp used was previously reported by our research group [18]. A continuous flow (1 mL min^{-1}) was maintained during the reaction. The products were monitored using gas and liquid chromatography by Thermo Scientific Trace 1310 and Shimadzu Prominence-i LC-2030C model.

Results

Characterization of the films

The morphology of the films was studied by Scanning Electron Microscopy. The mica substrate showed a smooth surface with negligible roughness while the reference perovskite exhibited a compact microstructure with a certain degree of agglomeration, as seen in Figures 2a and 2b. The bilayer films exhibited different microstructures showing that TiO_2 and ZnO do not favor a complete coverage of the perovskite (Figure 2, c-d). As in the case of TiO_2, some nanosheets were observed, which could be related to the presence of a partial decomposition of the base material [9].

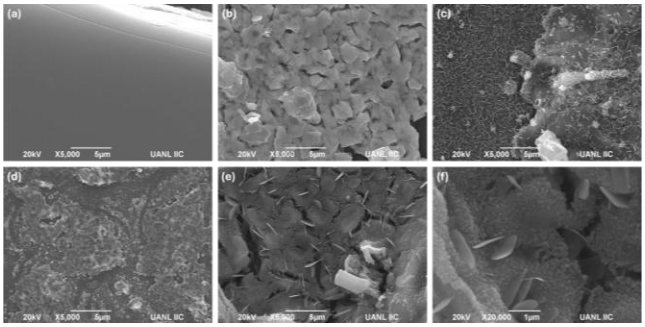

Figure 2. SEM images of (a) mica, (b) $K_3Bi_2I_9$, (c) $K_3Bi_2I_9/TiO_2$, (d) $K_3Bi_2I_9/ZnO$, and (e,f) $K_3Bi_2I_9/CuO$ films.

The CuO bilayer exhibited better coverage with small nanospheres that grew over the perovskite layers (Figure 2, e-f), which can benefit the photocatalytic reactions.

Figure 3 shows the absorption spectra of the different films, with different absorption bands observed for each sample. Notably, TiO_2 and ZnO showed absorption bands at higher wavelengths than usual, probably due to the absorption of the mica substrate. Although the simple oxides deposited on mica substrates absorb energy from 500 nm, showing their characteristic bands around 350 nm (TiO_2 and ZnO) and 700 nm (CuO). The absorption spectra of the bilayer films exhibited similar bands, as seen in Figure 3b. The band gap of the reference $K_3Bi_2I_9$ film was 1.9 eV, which agrees with previous reports (9), while the band edge of the reference film shifted to higher wavelengths, which evidenced an enhanced light absorption. This phenomenon was more evident in the $K_3Bi_2I_9/CuO$ film.

Figure 4 shows the XRD pattern of the substrate and the reference $K_3Bi_2I_9$ film. The substrate exhibited an intense and sharp reflection around 2θ ~ 10° associated with the muscovite phase (card 07–0042) of the mica. After the deposition of the $K_3Bi_2I_9$ film, a small reflection located ~ 13° in 2θ is associated with the monoclinic phase of this material. It is important to mention that the diffractogram of the bilayer films did not show additional reflections of the simple oxides, probably due to the low thickness of the film. Previous studies under similar experimental conditions have reported that metal oxide films with thicknesses below 100 nm typically yield signals too weak to be detected by XRD [19–22].

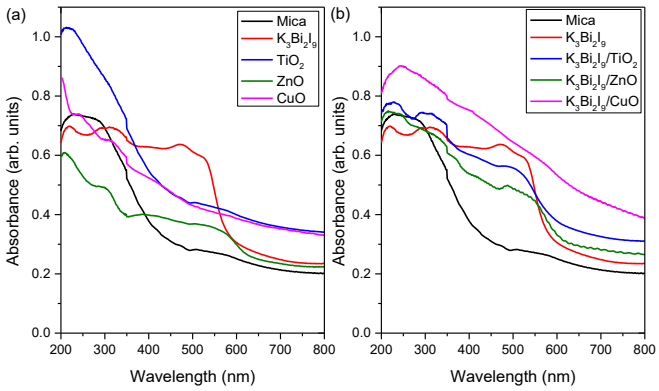

Figure 3. Absorption spectra of the (a) reference and (b) bilayer films grown on mica substrates.

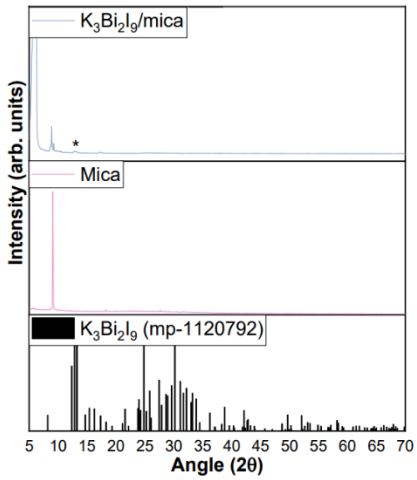

Figure 4. X-ray diffraction of the $K_3Bi_2I_9$ films on mica substrate.

Photocatalytic activity

The references and the bilayer films were evaluated as catalyst in CO_2 photoreduction at room conditions (298 K, 1 bar). Different products such as HCOOH, HCHO, CH_3OH, CH_4 and CO were monitored during this reaction, however, only formic acid was detected. Figure 5a shows the amount of formic acid generated after 1 h of reaction with the references.

To confirm the stability of each system, the evolution of HCOOH was monitored by one hour of reaction under visible-light irradiation. Figure 6a shows that the reference sample exhibited rapid activation; however, its efficiency for HCOOH production reached equilibrium faster than the other samples. On the contrary, the $K_3Bi_2I_9/CuO$ film exhibited a linear trend and a more constant fuel production, while the rest of the samples showed low activity. The reference and the bilayer film with the highest activity was evaluated in five consecutive cycles to observe changes and differences in the HCOOH yield. As shown in Figure 6b, the activity of the $K_3Bi_2I_9$ perovskite significantly decreased after the second cycle of evaluation, which confirms its low stability in aqueous medium under irradiation. Alternatively, despite the bilayer $K_3Bi_2I_9/CuO$ film shows lower activity than the bare sample, it exhibited a more stable production of formic acid. These results confirm that the construction of bilayer films is a suitable strategy to delay the degradation of the perovskite in an aqueous medium.

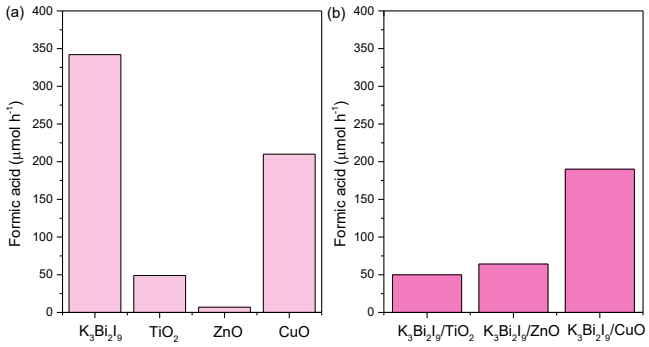

Figure 5. HCOOH production from CO_2 reduction using (a) references and (b) bilayer films under visible light. Catalyst area = 5 cm^2, mass < 0.01 g.

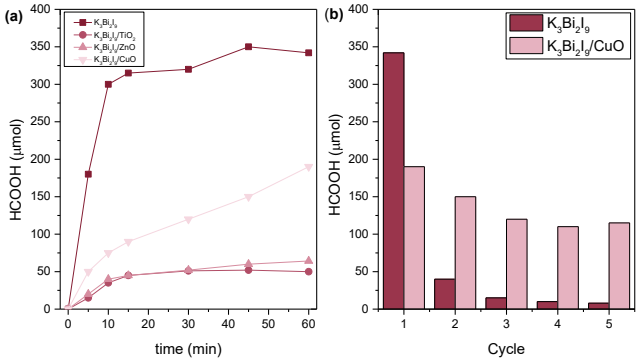

Figure 6. (a) Evolution of HCOOH production using the reference and bilayer films and (b) comparison of the HCOOH yield in 5 consecutive cycles of evaluation under visible light (area = 5 cm^2, mass < 0.01 g).

It is well recognized that rigorous control experiments are essential to rule out possible pseudo-catalytic contributions for the K_3Bi_2I9/CuO film. In this study, dark, and Ar-purged control experiments were performed to confirm that the observed activity arises from the films under illumination to validate the origin of the detected products. A clear signal was obtained only under CO_2 under irradiation, while negligible amounts were observed in the dark or under Ar atmosphere (< 20 μmol). These findings confirm that the detected formic acid arises from the photocatalytic CO_2 reduction process rather than from side reactions or impurities.

Discussion of the mechanism

The changes on the photocatalytic activity of the reference and bilayer films on the CO_2 reduction would be based on the band engineering of each oxide/halide. To support this hypothesis, the redox potentials of the conduction (CB) and valence bands (VB) were calculated theoretically and a charge transfer mechanism on each system are shown in Figure 8. When the oxides with wider band gaps, e.g., TiO_2 and ZnO, are used as window layers, the transfer of the photogenerated charges to the perovskite could be hindered due to the mismatch of the band structure between the semiconductors (Figure 8a). On the other hand, the $K_3Bi_2I_9$/CuO film presented a better match between the

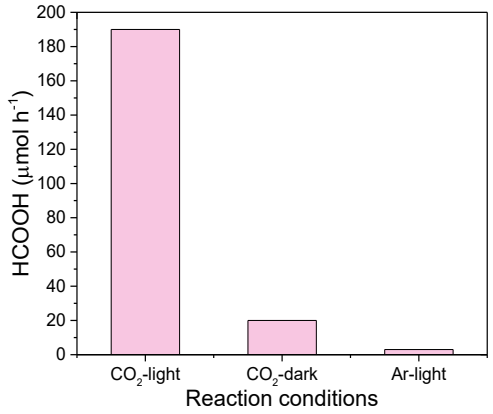

Figure 7. Control experiments (dark and Ar-purged) of the system with the best stability $K_3Bi_2I_9$/CuO film.

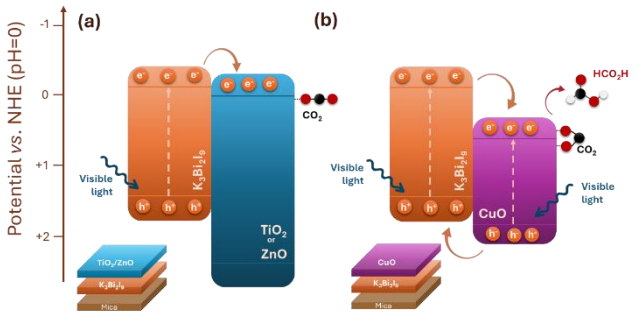

Figure 8. Proposed mechanism for CO_2 reduction using $K_3Bi_2I_9$ perovskites encapsulated with (a) ZnO or TiO_2 and (b) CuO oxides.

semiconductors, favoring the electron transfer from the perovskite CB to the oxide (CuO) CB; meanwhile, the holes can be transferred from the VB of CuO to the $K_3Bi_2I_9$ VB (Figure 8b). In addition, the surface characteristics of the CuO film may enhance CO_2 adsorption through uni- and bidentate bonds [23, 24]. This property could promote stronger interactions with CO_2 molecules, thereby facilitating higher conversions into value-added products, such as HCOOH.

The higher selectivity for formic acid generation from the photocatalytic CO_2 reduction using $K_3Bi_2I_9$ perovskite materials, particularly with the addition of CuO, can be attributed to several factors related to the properties of these materials:

- Perovskite materials, such as $K_3Bi_2I_9$, have unique structural characteristics that allow for the efficient adsorption and activation of CO_2; their crystal structure provides large proportion of low-coordinated metal atoms and thus, more active sites that promote the formation of low oxidation state products like formic acid [25]. These materials are known for stabilizing reaction intermediates that are critical for CO_2 reduction, which in turn favors the formation of two-electron process to produce HCOOH over other products [26].
- The addition of CuO to the perovskite was critical in enhancing the selectivity towards formic acid. Copper-based materials are widely studied for their ability to facilitate the conversion of CO_2 to formate ($HCOO^-$), which can then be protonated to form HCOOH [27]. The role of CuO in this system could be that of a co-catalyst, assisting in the adsorption of CO_2 and providing favorable conditions for the formation of formate intermediates compared to other products [28].
- The combination of $K_3Bi_2I_9$ and CuO likely results in a synergistic effect that enhances the overall photocatalytic performance and product selectivity. While the perovskite material facilitates CO_2 activation, CuO enhances the reduction process by stabilizing the intermediates and lowering the overpotentials associated with the reduction of CO_2 to formic acid [29]. This interaction not only improves the efficiency of the reduction but also ensures the stability of the catalyst during prolonged reaction times.

In summary, the enhanced selectivity towards HCOOH production in the photocatalytic CO_2 reduction using $K_3Bi_2I_9$

Table 1. Comparative analysis of HCOOH production using different photocatalytic systems (thin films and powders).

Photocatalytic system	Light source	Solvent	Efficiency (μmol h^{-1})	Stability (h)	Ref.
$NaTaO_3/Fe_2O_3$	UV light (254 nm)	Seawater	634	1	[30]
$K_3Bi_2I_9$	Visible light (λ > 400 nm), 20 W	H_2O	283	1	[9]
$KMgI_3$	Visible light (λ > 400 nm), 20 W	H_2O	68	NS	[31]
Ni-Cu_xO	Visible light (λ > 400 nm), 20 W	H_2O	15	NS	[32]
BiOI	Visible light (λ > 400 nm), 20 W	H_2O	14	5	[33]
Cu_2O/CuO	Visible light (λ > 400 nm), 20 W	H_2O	17	3	[34]
NH_2-C@Cu_2O	Visible light (λ > 420 nm), 300 W	Na_2SO_3	7	5 cycles	[35]
$Cs_2AgInCl_6$	UV light (380 nm), 5W	CH_3CN, H_2O, and H_2O/CH_3CN	3	2	[36]
$K_3Bi_2I_9/CuO$	Visible light (λ > 400 nm), 20 W	H_2O	190	5	*This work*

NS refers to not specified.

perovskite materials, particularly with the addition of CuO, can be explained by the unique properties of both materials.

Table 1 shows a comparative analysis of production of HCOOH from the photocatalytic CO_2 reduction. Compared to other reported photocatalytic systems, the $K_3Bi_2I_9/CuO$ film heterostructured exhibits notable advantages. First, it operates under visible-light irradiation (λ > 400 nm), in contrast to benchmark perovskite-based materials such as $NaTaO_3/Fe_2O_3$ or $Cs_2AgInCl_6$, which require UV light for its activation. Second, the hydrogen evolution rate (190 μmol h^{-1}) is significantly higher than that of other visible-light-driven systems, including BiOI (14 μmol h^{-1}), Cu_2O/CuO (17 μmol h^{-1}), and Ni–Cu_xO (15 μmol h^{-1}); although it was surpassed by pristine $K_3Bi_2I_9$ (283 μmol h^{-1}) its stability was significantly enhanced. Importantly, the heterostructure also demonstrates enhanced stability, maintaining activity for up to 5 h, which is considerably longer than the 1 h typically reported for single-component halides. These results suggest that coupling $K_3Bi_2I_9$ with CuO effectively improves the balance between photocatalytic activity and operational stability, making it a promising candidate among bismuth-based lead-free halides.

Conclusions

The stability of a lead-free metal halide perovskite for CO_2 photoreduction was controlled by a bilayer thin film of $K_3Bi_2I_9$/MO (M=Ti, Cu, Zn). The perovskites were grown on mica substrates by the spin-coating technique, and were covered by TiO_2, ZnO, and CuO oxides deposited by physical (sputtering) and chemical (atomic layer deposition) techniques. The incorporation of the simple oxides improves the light absorption and stability of the $K_3Bi_2I_9$ perovskite. Even though the film of $K_3Bi_2I_9$/MO (M=Cu, Zn) showed a decrease on performance due to the mismatch of the band in the bilayer film; it is necessary to note the benefit of giving stability to the halide perovskite, making it reusable and easy to recover. These strategies of encapsulation favored stability and efficiency of the bilayer, making a good alternative for a future optimization.

Acknowledgements

The authors thank SECIHTI for financial support of this research through the projects: Cátedras 1060 and Paradigmas y Fronteras de la Ciencia 320379. Also, the authors want to thank María Isabel Mendivil Palma for her support in the deposition of TiO_2 and ZnO films by the chemical methods.

References

[1]. S. Yoshino, T. Takayama, Y. Yamaguchi, I. Akihide, A. Kudo, *Acc. Chem. Res*. **55**, 966 (2022).
[2]. A. Mustafa, B.G. Lougou, Y. Shuai, Z. Wang, H. Tan, *J. Energy Chem.* **49**, 96 (2020).
[3]. G. Sahara, O. Ishitani, *Inorg. Chem*. **54**, 5096 (2015).
[4]. S. Zeng, P. Kar, U.K. Thakur, K. Shankar, *Nanotechnology* **29**, 052001 (2018).
[5]. M.A. Raza, F. Li, M. Que, L. Zhu, X. Chen, *Mater. Adv.* **2**, 7187 (2021).
[6]. X. Fu, T. Ren, S. Jiao, Z. Tian, J. Yang, Q. Li, *J. Energy Chem.* **83**, 397 (2023).
[7]. Z. Chen, Y. Hu, Y. Wang, Q. Shen, Y. Zhang, C. Ding, Y. Bai, G. Jiang, Z. Li, N. Gaponik, *Chem. Mater.* **32**, 1517 (2020).
[8]. E. Luévano-Hipólito, O.L. Quintero-Lizárraga, L.M. Torres-Martínez, *Catalysts* **12**, 1410 (2022).
[9]. O.L. Quintero-Lizárraga, E. Luévano-Hipólito, L.I. Ibarra-Rodríguez, L.M. Torres-Martínez, *Sustainability* **15**, 16835 (2023).
[10]. S. Chu, Y. Wang, Y. Guo, J. Feng, C. Wang, W. Luo, X. Fan, Z. Zou, *ACS Catal.* **3**, 912 (2013).
[11]. Z.L. Liu, R.R. Liu, Y.F. Mu, Y.X. Feng, G.X. Dong, M. Zhang, T.B. Lu, *Sol. RRL* **5**, 2000691 (2021).
[12]. Y.X. Feng, G.X. Dong, K. Su, Z.L. Liu, W. Zhang, M. Zhang, T.B. Lu, *J. Energy Chem.* **69**, 348 (2022).

[13]. Z. Zhang, M. Wang, Z. Chi, W. Li, H. Yu, N. Yang, H. Yu, *Appl. Catal. B* **313**, 121426 (2022).
[14]. Q.M. Sun, J.J. Xu, F.F. Tao, W. Ye, C. Zhou, J.H. He, J.M. Lu, *Angew. Chem.* **134**, e202200872 (2022).
[15]. D. Li, Z. Xing, X. Meng, X. Hu, T. Hu, Y. Chen, *Nano Lett.* **23**, 3484 (2023).
[16]. R. Dash, C. Mahender, P.K. Sahoo, A. Soam, *Mater. Today* **41**, 161 (2021).
[17]. A.E. Nogueira, G.T.S.T. da Silva, J.A. Oliveira, J.A. Torres, M.G.S. da Silva, M. Carmo, C. Ribeiro, *Catal. Commun.* **137**, 105929 (2020).
[18]. E. Luévano-Hipólito, L.M. Torres-Martínez, *Mat. Sci. Eng. B* **226**, 223 (2017).
[19]. M.R. Alfaro Cruz, O. Ceballos-Sanchez, E. Luévano-Hipólito, L.M. Torres-Martínez, *Int. J. Hydrogen Energy* **43**, 10301 (2018).
[20]. M.R. Alfaro Cruz, D. Sanchez-Martinez, L.M. Torres-Martínez, *Mat. Res. Bull* **122**, 110678 (2020).
[21]. M.R. Alfaro Cruz, D. Sanchez-Martinez, L.M. Torres-Martínez, *Int. J. Hydrogen Energy* **44**, 20017 (2019).
[22]. J.R. Castillo-Saenz, N. Nedev, B. Valdez-Salas, M.A. Martinez-Puente, F.S. Aguirre-Tostado, M.I. Mendivil-Palma, D. Mateos, M.A. Curiel-Alvarez, O. Perez-Landeros, E. Martinez-Guerra, *J. Mater. Sci.: Mater. Electron* **32**, 20274 (2021).
[23]. M.A. Ávila-López, E. Luévano-Hipólito, L.M. Torres-Martínez, *J. Photochem. Photobiol. A* **382**, 111933 (2019).
[24]. W.N.R.W. Isahak, Z.A.C. Ramli, M.W. Ismail, K. Ismail, R.M. Yusop, M.W.M. Hisham, M.A. Yarmo, *J. CO_2 Util.* **2**, 8 (2013).
[25]. H. Liu, S. Bansal, *Mater. Today Energy* **32**, 101230 (2023).
[26]. Z. Dong, B. Li, Y. Zhu, W. Guo, *EES Catalysis* **2**, 448 (2024).
[27]. D. Liu, Y. Hu, E. Shoko, H. Yu, T.T. Isimjan, X. Yang, *Electrochim. Acta* **365**, 137343 (2021).
[28]. S.A. Al-Tamreh, M.H. Ibrahim, M.H. El-Naas, J. Vaes, D. Pant, A. Benamor, A. Amhamed, "Electroreduction of Carbon Dioxide into Formate: A Comprehensive Review", *ChemElectroChem* **8**, 3207 (2021).
[29]. L.J. Minggu, M.N.I. Salehmin, M.A. Mohamed, K. Arifin, R.M. Yunus, M.B. Kassim, *Ceram. Int* **46**, 26004 (2020).
[30]. E. Luévano-Hipólito, A. Aguirre-Astrain, L.M. Torres-Martínez, *Mater. Sci. Semicond. Proc* **185**, 108984 (2025).
[31]. E. Luévano-Hipólito, M.G. Fabela-Cedillo, L.M. Torres-Martínez, *Mat. Lett* **361**, 136066 (2024).
[32]. L.I. Ibarra-Rodriguez, M.R. Alfaro Cruz, L.F. Garay-Rodriguez, B.C. Hernandez-Majalca, J.L. Domínguez-Arvizu, A. López-Ortiz, L.M. Torres-Martínez, V.H. Collins-Martínez, *J. Mater. Res. Technol* **26**, 137 (2023).
[33]. E. Luévano-Hipólito, D.A. Torres-Alvarez, L.M. Torres-Martínez, *J. Environ. Chem. Eng.* **11**, 109557 (2023).
[34]. E. Luévano-Hipólito, L.M. Torres-Martínez, M.A. Ávila-López, *J. Phys. Chem. Solids* **170**, 110924 (2022).
[35]. Q. Zhu, Y. Cao, Y. Tao, T. Li, Y. Zhang, H. Shang, J. Song, G. Li, *J. CO_2 Util.* **54**, 101781 (2021).
[36]. A. Kaliyaperumal, A.V. Gopala, G. Pandurangappa, B.R.K. Nanda, R. Chetty, A.K. Chandiran, *ACS Appl. Mater. Interfaces* **17**, 13896 (2025).